https://doi.org/10.3847/1538-4357/ab7afb

ANTARES and IceCube Combined Search for Neutrino Point-like and Extended Sources in the Southern Sky

A. Albert[1,2], M. André[3], M. Anghinolfi[4], G. Anton[5], M. Ardid[6], J.-J. Aubert[7], J. Aublin[8], B. Baret[8], S. Basa[9], B. Belhorma[10], V. Bertin[7], S. Biagi[11], M. Bissinger[5], J. Boumaaza[12], S. Bourret[8], M. Bouta[13], M. C. Bouwhuis[14], H. Brânzaş[15], R. Bruijn[14,16], J. Brunner[7], J. Busto[7], A. Capone[17,18], L. Caramete[15], J. Carr[7], S. Celli[17,18,19], M. Chabab[20], T. N. Chau[8], R. Cherkaoui El Moursli[12], T. Chiarusi[21], M. Circella[22], A. Coleiro[8], M. Colomer[8,23], R. Coniglione[11], H. Costantini[7], P. Coyle[7], A. Creusot[8], A. F. Díaz[24], G. de Wasseige[8], A. Deschamps[25], C. Distefano[11], I. Di Palma[17,18], A. Domi[4,26], C. Donzaud[8,27], D. Dornic[7], D. Drouin[1,2], T. Eberl[5], I. El Bojaddaini[13], N. El Khayati[12], D. Elsässer[28], A. Enzenhöfer[5,7], A. Ettahiri[12], F. Fassi[12], P. Fermani[17,18], G. Ferrara[11], F. Filippini[21,29], L. Fusco[8,29], P. Gay[8,30], H. Glotin[31], R. Gozzini[23], R. Gracia Ruiz[1], K. Graf[5], C. Guidi[4,26], S. Hallmann[5], H. van Haren[32], A. J. Heijboer[14], Y. Hello[25], J. J. Hernández-Rey[23], J. Hößl[5], J. Hofestädt[5], G. Illuminati[23], C. W. James[33], M. de Jong[14,34], P. de Jong[14], M. Jongen[14], M. Kadler[28], O. Kalekin[5], U. Katz[5], N. R. Khan-Chowdhury[23], A. Kouchner[8,35], M. Kreter[28], I. Kreykenbohm[36], V. Kulikovskiy[4,37], R. Lahmann[5], R. Le Breton[8], D. Lefèvre[38,39], E. Leonora[40], G. Levi[21,29], M. Lincetto[7], D. Lopez-Coto[41], S. Loucatos[8,42], G. Maggi[7], J. Manczak[23], M. Marcelin[9], A. Margiotta[21,29], A. Marinelli[43,44], J. A. Martínez-Mora[6], R. Mele[45,46], K. Melis[14,16], P. Migliozzi[45], M. Moser[5], A. Moussa[13], R. Muller[14], L. Nauta[14], S. Navas[41], E. Nezri[9], C. Nielsen[8], A. Nuñez-Castiñeyra[7,9], B. O'Fearraigh[14], M. Organokov[1], G. E. Păvălaş[15], C. Pellegrino[21,29], M. Perrin-Terrin[7], P. Piattelli[11], C. Poirè[6], V. Popa[15], T. Pradier[1], L. Quinn[7], N. Randazzo[40], G. Riccobene[11], A. Sánchez-Losa[22], A. Salah-Eddine[20], D. F. E. Samtleben[14,34], M. Sanguineti[4,26], P. Sapienza[11], F. Schüssler[42], M. Spurio[21,29], Th. Stolarczyk[42], B. Strandberg[14], M. Taiuti[4,26], Y. Tayalati[12], T. Thakore[23], S. J. Tingay[33], A. Trovato[11], B. Vallage[8,42], V. Van Elewyck[8,35], F. Versari[8,21,29], S. Viola[11], D. Vivolo[45,46], J. Wilms[36], D. Zaborov[7], A. Zegarelli[17,18], J. D. Zornoza[23], J. Zúñiga[23]

(ANTARES Collaboration),

and

M. G. Aartsen[47], M. Ackermann[48], J. Adams[47], J. A. Aguilar[49], M. Ahlers[50], M. Ahrens[51], C. Alispach[52], K. Andeen[53], T. Anderson[54], I. Ansseau[49], G. Anton[55], C. Argüelles[56], J. Auffenberg[57], S. Axani[56], P. Backes[57], H. Bagherpour[47], X. Bai[58], A. Balagopal V.[59], A. Barbano[52], S. W. Barwick[60], B. Bastian[48], V. Baum[61], S. Baur[49], R. Bay[62], J. J. Beatty[63,64], K.-H. Becker[65], J. Becker Tjus[66], S. BenZvi[67], D. Berley[68], E. Bernardini[48,102], D. Z. Besson[69,103], G. Binder[62,70], D. Bindig[65], E. Blaufuss[68], S. Blot[48], C. Bohm[51], S. Böser[61], O. Botner[71], J. Böttcher[57], E. Bourbeau[50], J. Bourbeau[72], F. Bradascio[48], J. Braun[72], S. Bron[52], J. Brostean-Kaiser[48], A. Burgman[71], J. Buscher[57], R. S. Busse[73], T. Carver[52], C. Chen[74], E. Cheung[68], D. Chirkin[72], S. Choi[75], K. Clark[76], L. Classen[73], A. Coleman[77], G. H. Collin[56], J. M. Conrad[56], P. Coppin[78], P. Correa[78], D. F. Cowen[54,79], R. Cross[67], P. Dave[74], C. De Clercq[78], J. J. DeLaunay[54], H. Dembinski[77], K. Deoskar[51], S. De Ridder[80], P. Desiati[72], K. D. de Vries[78], G. de Wasseige[78], M. de With[81], T. DeYoung[82], A. Diaz[56], J. C. Díaz-Vélez[72], H. Dujmovic[59], M. Dunkman[54], E. Dvorak[58], B. Eberhardt[72], T. Ehrhardt[61], P. Eller[54], R. Engel[59], P. A. Evenson[77], S. Fahey[72], A. R. Fazely[83], J. Felde[68], K. Filimonov[62], C. Finley[51], D. Fox[79], A. Franckowiak[48], E. Friedman[68], A. Fritz[61], T. K. Gaisser[77], J. Gallagher[84], E. Ganster[57], S. Garrappa[48], L. Gerhardt[70], K. Ghorbani[72], T. Glauch[85], T. Glüsenkamp[55], A. Goldschmidt[70], J. G. Gonzalez[77], D. Grant[82], T. Grégoire[54], Z. Griffith[72], S. Griswold[67], M. Günder[57], M. Gündüz[66], C. Haack[57], A. Hallgren[71], R. Halliday[82], L. Halve[57], F. Halzen[72], K. Hanson[72], A. Haungs[59], D. Hebecker[81], D. Heereman[49], P. Heix[57], K. Helbing[65], R. Hellauer[68], F. Henningsen[85], S. Hickford[65], J. Hignight[86], G. C. Hill[87], K. D. Hoffman[68], R. Hoffmann[65], T. Hoinka[88], B. Hokanson-Fasig[72], K. Hoshina[72,104], F. Huang[54], M. Huber[85], T. Huber[48,59], K. Hultqvist[51], M. Hünnefeld[88], R. Hussain[72], S. In[75], N. Iovine[49], A. Ishihara[89], M. Jansson[51], G. S. Japaridze[90], M. Jeong[75], K. Jero[72], B. J. P. Jones[91], F. Jonske[57], R. Joppe[57], D. Kang[59], W. Kang[75], A. Kappes[73], D. Kappesser[61], T. Karg[48], M. Karl[85], A. Karle[72], U. Katz[55], M. Kauer[72], J. L. Kelley[72], A. Kheirandish[72], J. Kim[75], T. Kintscher[48], J. Kiryluk[92], T. Kittler[55], S. R. Klein[62,70], R. Koirala[77], H. Kolanoski[81], L. Köpke[61], C. Kopper[82], S. Kopper[93], D. J. Koskinen[50], M. Kowalski[48,81], K. Krings[85], G. Krückl[61], N. Kulacz[86], N. Kurahashi[94], A. Kyriacou[87], J. L. Lanfranchi[54], M. J. Larson[68], F. Lauber[65], J. P. Lazar[72], K. Leonard[72], A. Leszczyńska[59], M. Leuermann[57], Q. R. Liu[72], E. Lohfink[61], C. J. Lozano Mariscal[73], L. Lu[89], F. Lucarelli[52], J. Lünemann[78], W. Luszczak[72], Y. Lyu[62,70], W. Y. Ma[48], J. Madsen[95], G. Maggi[78], K. B. M. Mahn[82], Y. Makino[89], P. Mallik[57], K. Mallot[72], S. Mancina[72], I. C. Mariş[49], R. Maruyama[96], K. Mase[89], R. Maunu[68], F. McNally[97], K. Meagher[72], M. Medici[50], A. Medina[64], M. Meier[88], S. Meighen-Berger[85], G. Merino[72], T. Meures[49], J. Micallef[82], D. Mockler[49], G. Momenté[61], T. Montaruli[52], R. W. Moore[86], R. Morse[72], M. Moulai[56], P. Muth[57], R. Nagai[89], U. Naumann[65], G. Neer[82], H. Niederhausen[85], M. U. Nisa[82], S. C. Nowicki[82], D. R. Nygren[70], A. Obertacke Pollmann[65], M. Oehler[59], A. Olivas[68], A. O'Murchadha[49], E. O'Sullivan[51], T. Palczewski[62,70], H. Pandya[77], D. V. Pankova[54], N. Park[72], P. Peiffer[61], C. Pérez de los Heros[71], S. Philippen[57], D. Pieloth[88], S. Pieper[65], E. Pinat[49], A. Pizzuto[72], M. Plum[53], A. Porcelli[80], P. B. Price[62], G. T. Przybylski[70], C. Raab[49], A. Raissi[47], M. Rameez[50], L. Rauch[48], K. Rawlins[98], I. C. Rea[85], R. Reimann[57], B. Relethford[94], M. Renschler[59], G. Renzi[49], E. Resconi[85], W. Rhode[88], M. Richman[94], S. Robertson[70], M. Rongen[57], C. Rott[75], T. Ruhe[88], D. Ryckbosch[80], D. Rysewyk[82], I. Safa[72], S. E. Sanchez Herrera[82], A. Sandrock[88], J. Sandroos[61], M. Santander[93], S. Sarkar[99], S. Sarkar[86], K. Satalecka[48], M. Schaufel[57], H. Schieler[59], P. Schlunder[88], T. Schmidt[68], A. Schneider[72], J. Schneider[55],

F. G. Schröder[59,77], L. Schumacher[57], S. Sclafani[94], D. Seckel[77], S. Seunarine[95], S. Shefali[57], M. Silva[72], R. Snihur[72],
J. Soedingrekso[88], D. Soldin[77], M. Song[68], G. M. Spiczak[95], C. Spiering[48], J. Stachurska[48], M. Stamatikos[64], T. Stanev[77],
R. Stein[48], J. Stettner[57], A. Steuer[61], T. Stezelberger[70], R. G. Stokstad[70], A. Stößl[89], N. L. Strotjohann[48], T. Stürwald[57],
T. Stuttard[50], G. W. Sullivan[68], I. Taboada[74], F. Tenholt[66], S. Ter-Antonyan[83], A. Terliuk[48], S. Tilav[77], K. Tollefson[82],
L. Tomankova[66], C. Tönnis[100], S. Toscano[49], D. Tosi[72], A. Trettin[48], M. Tselengidou[55], C. F. Tung[74], A. Turcati[85], R. Turcotte[59],
C. F. Turley[54], B. Ty[72], E. Unger[71], M. A. Unland Elorrieta[73], M. Usner[48], J. Vandenbroucke[72], W. Van Driessche[80], D. van Eijk[72],
N. van Eijndhoven[78], J. van Santen[48], S. Verpoest[80], M. Vraeghe[80], C. Walck[51], A. Wallace[87], M. Wallraff[57], N. Wandkowsky[72],
T. B. Watson[91], C. Weaver[86], A. Weindl[59], M. J. Weiss[54], J. Weldert[61], C. Wendt[72], J. Werthebach[72], B. J. Whelan[87],
N. Whitehorn[101], K. Wiebe[61], C. H. Wiebusch[57], L. Wille[72], D. R. Williams[93], L. Wills[94], M. Wolf[85], J. Wood[72], T. R. Wood[86],
K. Woschnagg[62], G. Wrede[55], D. L. Xu[72], X. W. Xu[83], Y. Xu[92], J. P. Yanez[86], G. Yodh[60], S. Yoshida[89], T. Yuan[72], and
M. Zöcklein[57]
(IceCube Collaboration)
[1] Université de Strasbourg, CNRS, IPHC UMR 7178, F-67000 Strasbourg, France
[2] Université de Haute Alsace, F-68200 Mulhouse, France
[3] Technical University of Catalonia, Laboratory of Applied Bioacoustics, Rambla Exposició, E-08800 Vilanova i la Geltrú, Barcelona, Spain
[4] INFN—Sezione di Genova, Via Dodecaneso 33, I-16146 Genova, Italy
[5] Friedrich-Alexander-Universität Erlangen-Nürnberg, Erlangen Centre for Astroparticle Physics, Erwin-Rommel-Str. 1, D-91058 Erlangen, Germany
[6] Institut d'Investigació per a la Gestió Integrada de les Zones Costaneres (IGIC)—Universitat Politècnica de València. C/Paranimf 1, E-46730 Gandia, Spain
[7] Aix Marseille Univ, CNRS/IN2P3, CPPM, Marseille, France
[8] APC, Univ Paris Diderot, CNRS/IN2P3, CEA/Irfu, Obs de Paris, Sorbonne Paris Cité, France
[9] Aix Marseille Univ, CNRS, CNES, LAM, Marseille, France
[10] National Center for Energy Sciences and Nuclear Techniques, B.P. 1382, R.P. 10001 Rabat, Morocco
[11] INFN—Laboratori Nazionali del Sud (LNS), Via S. Sofia 62, I-95123 Catania, Italy
[12] University Mohammed V in Rabat, Faculty of Sciences, 4 av. Ibn Battouta, B.P. 1014, R.P. 10000, Morocco
[13] University Mohammed I, Laboratory of Physics of Matter and Radiations, B.P. 717, Oujda 6000, Morocco
[14] Nikhef, Science Park, Amsterdam, The Netherlands
[15] Institute of Space Science, RO-077125 Bucharest, Măgurele, Romania
[16] Universiteit van Amsterdam, Instituut voor Hoge-Energie Fysica, Science Park 105, 1098 XG Amsterdam, The Netherlands
[17] INFN—Sezione di Roma, P.le Aldo Moro 2, I-00185 Roma, Italy
[18] Dipartimento di Fisica dell'Università La Sapienza, P.le Aldo Moro 2, I-00185 Roma, Italy
[19] Gran Sasso Science Institute, Viale Francesco Crispi 7, I-00167 L'Aquila, Italy
[20] LPHEA, Faculty of Science—Semlali, Cadi Ayyad University, P.O.B. 2390, Marrakech, Morocco
[21] INFN—Sezione di Bologna, Viale Berti-Pichat 6/2, I-40127 Bologna, Italy
[22] INFN—Sezione di Bari, Via E. Orabona 4, I-70126 Bari, Italy
[23] IFIC—Instituto de Física Corpuscular (CSIC—Universitat de València), c/ Catedrático José Beltrán, 2 E-46980 Paterna, Valencia, Spain; antares.spokesperson@in2p3.fr
[24] Dept. of Computer Architecture and Technology/CITIC, University of Granada, E-18071 Granada, Spain
[25] Géoazur, UCA, CNRS, IRD, Observatoire de la Côte d'Azur, Sophia Antipolis, France
[26] Dipartimento di Fisica dell'Università, Via Dodecaneso 33, I-16146 Genova, Italy
[27] Université Paris-Sud, F-91405 Orsay Cedex, France
[28] Institut für Theoretische Physik und Astrophysik, Universität Würzburg, Emil-Fischer Str. 31, D-97074 Würzburg, Germany
[29] Dipartimento di Fisica e Astronomia dell'Università, Viale Berti Pichat 6/2, I-40127 Bologna, Italy
[30] Laboratoire de Physique Corpusculaire, Clermont Université, Université Blaise Pascal, CNRS/IN2P3, BP 10448, F-63000 Clermont-Ferrand, France
[31] LIS, UMR Université de Toulon, Aix Marseille Université, CNRS, F-83041 Toulon, France
[32] Royal Netherlands Institute for Sea Research (NIOZ) and Utrecht University, Landsdiep 4, 1797 SZ 't Horntje (Texel), The Netherlands
[33] International Centre for Radio Astronomy Research—Curtin University, Bentley, WA 6102, Australia
[34] Huygens–Kamerlingh Onnes Laboratorium, Universiteit Leiden, The Netherlands
[35] Institut Universitaire de France, F-75005 Paris, France
[36] Dr. Remeis-Sternwarte and ECAP, Friedrich-Alexander-Universität Erlangen-Nürnberg, Sternwartstr. 7, D-96049 Bamberg, Germany
[37] Moscow State University, Skobeltsyn Institute of Nuclear Physics, Leninskie gory, 119991 Moscow, Russia
[38] Mediterranean Institute of Oceanography (MIO), Aix-Marseille University, F-13288, Marseille, Cedex 9, France
[39] Université du Sud Toulon-Var, CNRS-INSU/IRD UM 110, F-83957, La Garde Cedex, France
[40] INFN—Sezione di Catania, Via S. Sofia 64, I-95123 Catania, Italy
[41] Dpto. de Física Teórica y del Cosmos & C.A.F.P.E., University of Granada, E-18071 Granada, Spain
[42] IRFU, CEA, Université Paris-Saclay, F-91191 Gif-sur-Yvette, France
[43] INFN—Sezione di Pisa, Largo B. Pontecorvo 3, I-56127 Pisa, Italy
[44] Dipartimento di Fisica dell'Università, Largo B. Pontecorvo 3, I-56127 Pisa, Italy
[45] INFN—Sezione di Napoli, Via Cintia I-80126 Napoli, Italy
[46] Dipartimento di Fisica dell'Università Federico II di Napoli, Via Cintia I-80126, Napoli, Italy
[47] Dept. of Physics and Astronomy, University of Canterbury, Private Bag 4800, Christchurch, New Zealand
[48] DESY, D-15738 Zeuthen, Germany
[49] Université Libre de Bruxelles, Science Faculty CP230, B-1050 Brussels, Belgium
[50] Niels Bohr Institute, University of Copenhagen, DK-2100 Copenhagen, Denmark
[51] Oskar Klein Centre and Dept. of Physics, Stockholm University, SE-10691 Stockholm, Sweden
[52] Département de physique nucléaire et corpusculaire, Université de Genève, CH-1211 Genève, Switzerland
[53] Dept. of Physics, Marquette University, Milwaukee, WI 53201, USA
[54] Dept. of Physics, Pennsylvania State University, University Park, PA 16802, USA
[55] Erlangen Centre for Astroparticle Physics, Friedrich-Alexander-Universität Erlangen-Nürnberg, D-91058 Erlangen, Germany
[56] Dept. of Physics, Massachusetts Institute of Technology, Cambridge, MA 02139, USA
[57] III. Physikalisches Institut, RWTH Aachen University, D-52056 Aachen, Germany
[58] Physics Department, South Dakota School of Mines and Technology, Rapid City, SD 57701, USA
[59] Karlsruhe Institute of Technology, Institut für Kernphysik, D-76021 Karlsruhe, Germany
[60] Dept. of Physics and Astronomy, University of California, Irvine, CA 92697, USA
[61] Institute of Physics, University of Mainz, Staudinger Weg 7, D-55099 Mainz, Germany

[62] Dept. of Physics, University of California, Berkeley, CA 94720, USA

[63] Dept. of Astronomy, Ohio State University, Columbus, OH 43210, USA

[64] Dept. of Physics and Center for Cosmology and Astro-Particle Physics, Ohio State University, Columbus, OH 43210, USA

[65] Dept. of Physics, University of Wuppertal, D-42119 Wuppertal, Germany

[66] Fakultät für Physik & Astronomie, Ruhr-Universität Bochum, D-44780 Bochum, Germany

[67] Dept. of Physics and Astronomy, University of Rochester, Rochester, NY 14627, USA

[68] Dept. of Physics, University of Maryland, College Park, MD 20742, USA

[69] Dept. of Physics and Astronomy, University of Kansas, Lawrence, KS 66045, USA

[70] Lawrence Berkeley National Laboratory, Berkeley, CA 94720, USA

[71] Dept. of Physics and Astronomy, Uppsala University, Box 516, SE-75120 Uppsala, Sweden

[72] Dept. of Physics and Wisconsin IceCube Particle Astrophysics Center, University of Wisconsin, Madison, WI 53706, USA; analysis@icecube.wis.edu

[73] Institut für Kernphysik, Westfälische Wilhelms-Universität Münster, D-48149 Münster, Germany

[74] School of Physics and Center for Relativistic Astrophysics, Georgia Institute of Technology, Atlanta, GA 30332, USA

[75] Dept. of Physics, Sungkyunkwan University, Suwon 16419, Republic of Korea

[76] SNOLAB, 1039 Regional Road 24, Creighton Mine 9, Lively, ON, P3Y 1N2, Canada

[77] Bartol Research Institute and Dept. of Physics and Astronomy, University of Delaware, Newark, DE 19716, USA

[78] Vrije Universiteit Brussel (VUB), Dienst ELEM, B-1050 Brussels, Belgium

[79] Dept. of Astronomy and Astrophysics, Pennsylvania State University, University Park, PA 16802, USA

[80] Dept. of Physics and Astronomy, University of Gent, B-9000 Gent, Belgium

[81] Institut für Physik, Humboldt-Universität zu Berlin, D-12489 Berlin, Germany

[82] Dept. of Physics and Astronomy, Michigan State University, East Lansing, MI 48824, USA

[83] Dept. of Physics, Southern University, Baton Rouge, LA 70813, USA

[84] Dept. of Astronomy, University of Wisconsin, Madison, WI 53706, USA

[85] Physik-department, Technische Universität München, D-85748 Garching, Germany

[86] Dept. of Physics, University of Alberta, Edmonton, Alberta, T6G 2E1, Canada

[87] Dept. of Physics, University of Adelaide, Adelaide, 5005, Australia

[88] Dept. of Physics, TU Dortmund University, D-44221 Dortmund, Germany

[89] Dept. of Physics and Institute for Global Prominent Research, Chiba University, Chiba 263-8522, Japan

[90] CTSPS, Clark-Atlanta University, Atlanta, GA 30314, USA

[91] Dept. of Physics, University of Texas at Arlington, 502 Yates St., Science Hall Rm 108, Box 19059, Arlington, TX 76019, USA

[92] Dept. of Physics and Astronomy, Stony Brook University, Stony Brook, NY 11794-3800, USA

[93] Dept. of Physics and Astronomy, University of Alabama, Tuscaloosa, AL 35487, USA

[94] Dept. of Physics, Drexel University, 3141 Chestnut Street, Philadelphia, PA 19104, USA

[95] Dept. of Physics, University of Wisconsin, River Falls, WI 54022, USA

[96] Dept. of Physics, Yale University, New Haven, CT 06520, USA

[97] Dept. of Physics, Mercer University, Macon, GA 31207-0001, USA

[98] Dept. of Physics and Astronomy, University of Alaska Anchorage, 3211 Providence Dr., Anchorage, AK 99508, USA

[99] Dept. of Physics, University of Oxford, Parks Road, Oxford OX1 3PU, UK

[100] Institute of Basic Science, Sungkyunkwan University, Suwon 16419, Republic of Korea

[101] Dept. of Physics and Astronomy, UCLA, Los Angeles, CA 90095, USA

Abstract

A search for point-like and extended sources of cosmic neutrinos using data collected by the ANTARES and IceCube neutrino telescopes is presented. The data set consists of all the track-like and shower-like events pointing in the direction of the Southern Sky included in the nine-year ANTARES point-source analysis, combined with the throughgoing track-like events used in the seven-year IceCube point-source search. The advantageous field of view of ANTARES and the large size of IceCube are exploited to improve the sensitivity in the Southern Sky by a factor of ∼2 compared to both individual analyses. In this work, the Southern Sky is scanned for possible excesses of spatial clustering, and the positions of preselected candidate sources are investigated. In addition, special focus is given to the region around the Galactic Center, whereby a dedicated search at the location of SgrA* is performed, and to the location of the supernova remnant RXJ 1713.7-3946. No significant evidence for cosmic neutrino sources is found, and upper limits on the flux from the various searches are presented.

Unified Astronomy Thesaurus concepts: Neutrino astronomy (1100)

1. Introduction

Neutrinos are stable, neutral, and weakly interacting particles and, in contrast to cosmic rays, they are not deflected by magnetic fields. Differently from high-energy photons, neutrinos are effectively not absorbed while traveling through cosmological distances and can escape from dense astrophysical environments. These qualities make them ideal cosmic messengers as they point back to their production sites. Several classes of astrophysical objects, such as supernova remnants, pulsar wind nebulae, and active galactic nuclei (AGNs) have been indicated as promising high-energy neutrino source candidates (Gaisser et al. 1995; Halzen & Hooper 2002; Becker 2008; Kelner & Aharonian 2008; Murase 2015). Neutrinos are expected to be produced through the decay of charged mesons, a result of hadronic interactions of accelerated protons with matter or radiation in the surroundings of the acceleration sites.

Neutrino astronomy has recently entered an exciting period with the discovery of an isotropic high-energy cosmic neutrino

---

[102] Also at Università di Padova, I-35131 Padova, Italy.

[103] Also at National Research Nuclear University, Moscow Engineering Physics Institute (MEPhI), Moscow 115409, Russia.

[104] Also at Earthquake Research Institute, University of Tokyo, Bunkyo, Tokyo 113-0032, Japan.

flux reported in two groups of analyses by the IceCube Collaboration (Aartsen et al. 2014; Kopper et al. 2016; Kopper 2017, and Aartsen et al. 2016; Haack & Wiebusch 2017), followed by the first evidence of neutrino emission from an astrophysical source, the blazar TXS 0506+056 (Aartsen et al. 2018a, 2018b). These observations represent a major breakthrough in the field, and thus further investigations are strongly motivated. Indeed, the origin of most of the observed neutrino flux remains unknown. The neutrino flux of TXS 0506 +056 can only account for less than 1% of the total observed astrophysical flux (Aartsen et al. 2018a). Moreover, recent searches for neutrino emission from the directions of blazars in the second *Fermi*-LAT AGN catalog performed by the IceCube Collaboration indicated that blazars contribute less than about 40%–80% (30%) to the total observed neutrino flux, assuming an unbroken power-law spectrum $\Phi(E_\nu) \propto E_\nu^{-\gamma}$ with $\gamma = 2.0$ (Aartsen et al. 2018a) ($\gamma = 2.5$ (Aartsen et al. 2017a)). The region around TXS 0506+056 was studied also by the ANTARES Collaboration using data collected from 2007 to 2017 (Albert et al. 2018). The standard time-integrated method fits 1.03 signal events, which corresponds to a *p*-value of 3.4% (not considering trial corrections). These results encourage additional studies of potential neutrino sources, not only based on searches for a cumulative neutrino signal integrated over many years (such as the one presented here), but also relying on a time-dependent and/or multimessenger approach. Indeed, using the information of the neutrino arrival times is expected to significantly increase the discovery potential, as it improves the signal-to-background discrimination (Aartsen et al. 2015; Albert et al. 2019). Moreover, exploiting multimessenger observations helps to refine the selection of the target neutrino source candidates, allowing to reduce the number of tested locations and therefore the trial factor (Franckowiak 2017). However, if the hypothesis used to guide such searches is incorrect, sensitivity to neutrino sources will be reduced. Here, we present an untargeted search, to allow for the greatest range of possibilities.

In this work, the point-source data samples of the ANTARES (Ageron et al. 2011) and IceCube (Achterberg et al. 2006; Aartsen et al. 2017b) neutrino telescopes collected during nine (Adrian-Martinez et al. 2014) and seven years (Aartsen et al. 2017c), respectively, are combined to perform various searches for point-like and extended sources of neutrinos in the Southern Sky. This work supersedes a previous combined analysis using a smaller data sample of five and three years of ANTARES and IceCube data, respectively (Adrian-Martinez et al. 2016).

The two telescopes complement each other thanks to their different characteristics, in particular the larger instrumented volume of IceCube and the privileged view of the Southern Sky, with a reduced muon background for neutrino energies below 100 TeV of ANTARES. Exploiting these different characteristics allows for a significant gain in sensitivity for searches in the Southern Sky.

The paper is organized as follows. A brief description of the ANTARES and IceCube neutrino telescopes is given in Section 2. In Section 3, the samples employed in the searches are described. The analysis method and the expected performances are discussed in Section 4, while the performed searches and corresponding results are presented in Section 5. In Section 6, conclusions are drawn.

2. ANTARES and IceCube Neutrino Telescopes

The ANTARES and IceCube neutrino telescopes rely on the same principle for detecting cosmic neutrinos. A three-dimensional array of photomultiplier tubes (PMTs) inside a transparent medium—water or ice, respectively—collects the Cerenkov photons induced by the passage of relativistic charged particles. The charged particles are produced in neutrino interactions with the target medium, inside or near the instrumented volume. The information provided by the number of detected Cerenkov photons and their arrival times is used to infer the neutrino interaction topology, direction and energy.

The ANTARES telescope (Ageron et al. 2011) is located in the Mediterranean Sea, 40 km south of Toulon (France), at a depth of about 2400 m. It was completed in 2008, with the first lines operating since 2006. The detector comprises a three-dimensional array of 885 optical modules (OMs), each one housing a 10″ PMT, facing 45° downward in order to optimize the detection of Cerenkov photons from upgoing charged particles. The PMTs are distributed over 12 vertical lines with a length of 350 m, and with an interline separation between 60 and 75 m, instrumenting a total volume of ~ 0.01 km^3.

The IceCube telescope (Achterberg et al. 2006; Aartsen et al. 2017b) is a cubic-kilometer-sized detector located at the South Pole, between 1450 and 2450 m below the surface of the Antarctic ice. A total of 5160 digital optical modules (DOMs), each consisting of a pressure-resistant sphere that houses electronics, calibration LEDs, and a 10″ PMT facing downward, are attached to 86 vertical strings, with a mean distance between strings of ~ 125 m. The construction of the IceCube detector began in 2005 and was finished six years later. During the construction, data were collected with partial configurations of the detector, commonly indicated by ICXY, with XY denoting the number of active strings.

Two main event topologies can be identified in the ANTARES and IceCube telescopes: tracks and showers. Charged current (CC) interactions of muon neutrinos and antineutrinos produce a relativistic muon that can travel large distances through the medium, leaving a track-like signature in the detector. Shower-like events are induced by neutral current (NC) interactions, as well as by CC interactions of electron and tau neutrinos and antineutrinos, and are characterized by an almost spherically symmetric light emission around the shower maximum. The longer lever arm of the track topology allows for a better reconstruction of the particle direction and therefore for a better median angular resolution, while a better reconstruction of the particle energy is achieved for showers, as the topology allows for a calorimetric measurement.

Common backgrounds in both detectors are atmospheric muons and neutrinos originating from cosmic-ray interactions in Earth's atmosphere. Events from the Southern Sky correspond to downgoing events for IceCube. In this case, atmospheric muons represent the bulk of the detected events before selection, outnumbering the atmospheric neutrinos by a factor from 10^4 up to 10^6 depending on the direction. In contrast, ANTARES' detected events are predominantly atmospheric neutrinos because the Earth acts as a shield for atmospheric muons.
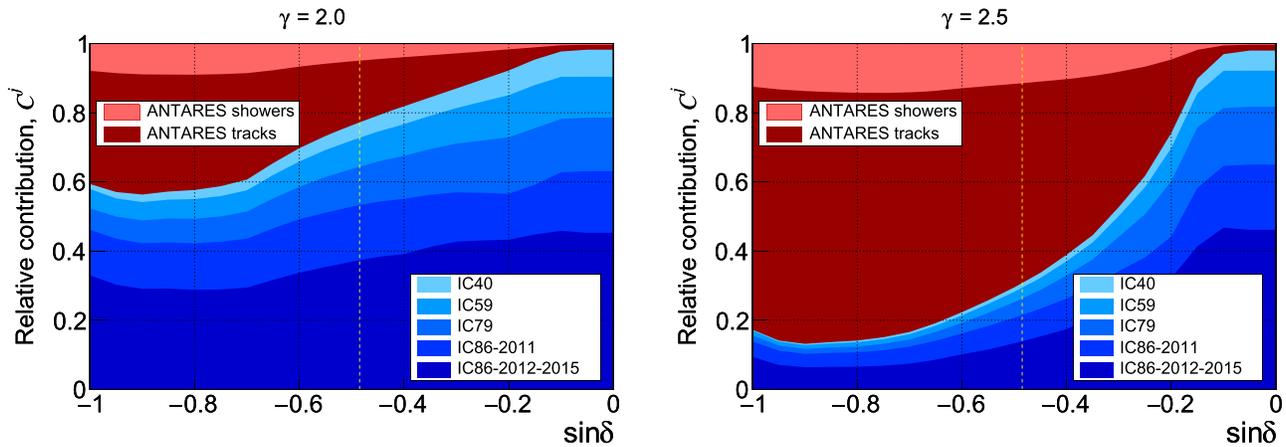
Figure 1. Relative contribution of each sample as a function of the source decl. for an unbroken $E_\nu^{-\gamma}$ spectrum, with $\gamma = 2.0$ (left) and $\gamma = 2.5$ (right). The contribution of the ANTARES (IceCube) samples is represented by different shades of red (blue). The vertical dashed line marks the decl. of the Galactic Center.

Table 1
ANTARES and IceCube Samples Used in This Analysis

ANTARES Sample	Index j	Livetime T (days)	Number of Events
Tracks	1	2415	5807
Showers	2	2415	102

IceCube Sample	Index j	Livetime T (days)	Number of Events
IC40	3	376	22779
IC59	4	348	64257
IC79	5	316	44771
IC86-2011	6	333	74931
IC86-2012-2015	7	1058	119231

Note. Overview of the seven data samples of ANTARES and IceCube employed in the analysis. Only Southern Sky events (numbers of events reported in the last column) have been selected for the present analysis.

3. Data Samples

All track-like and shower-like events from the Southern Sky that were employed in the nine-year ANTARES point-source analysis (Adrian-Martinez et al. 2014), combined with the throughgoing track-like events—i.e., tracks induced by muons traversing the detector—included in the seven-year IceCube point-source search (Aartsen et al. 2017c) are used in this analysis. The ANTARES data were collected between early 2007 and the end of 2015. The IceCube data were taken from 2008 to 2015, with the detector operating either in partial (samples IC40, IC59, IC79) or in full (samples IC86-2011, IC86-2012-2015) configuration.

Both the ANTARES and the IceCube event selection criteria were optimized to minimize the neutrino flux needed for a 5σ discovery of a point-like source emitting with a $E_\nu^{-2.0}$ spectrum.

The ANTARES events were selected by applying cuts on the zenith angle, the angular error estimate, and parameters describing the quality of the reconstruction. In the case of the shower events, a cut was also applied on the interaction vertex, required to be located within a fiducial volume slightly larger than the instrumented volume. A detailed description of these cuts can be found in Adrian-Martinez et al. (2014). A median angular resolution better than $0°.4$ is achieved for the selected tracks for energies above 100 TeV, and $\sim 3°$ for the selected showers for energies between 1 TeV and 0.5 PeV.

The IceCube selection of throughgoing tracks in the Southern Sky was based on multivariate selection techniques (boosted decision tree; BDT), which made use of parameters connected to the event quality, track topology, energy deposited along the track, and light-arrival time of photons at the DOMs (Aartsen et al. 2017c). This procedure selects only very high-energy events ($E_\nu \gtrsim 100$ TeV) with a median angular resolution better than $0°.4$ for energies above 1 PeV.

A summary of the data sets in terms of livetime and number of selected events in each sample and for each detector is given in Table 1.

As a consequence of the different layouts, locations of the telescopes and selection techniques in the Southern Sky, each sample has a different efficiency for detecting events from potential sources. The relative contribution $C^j(\delta, \Phi)$ for each sample j, defined as the ratio of the expected mean number of signal events for the given sample to that for all samples, $C^j = N^j / \sum_{i=1}^{7} N^i$, depends on the expected flux from the source Φ and decl. δ. For each ANTARES sample $j \in [1, 2]$ given in Table 1, the expected mean number of signal events, N^j, is obtained as (Aartsen et al. 2017c):

$$N^j = \sum_{f \in \{\mu, e, \tau\}} T^j \int d\Omega \int dE_\nu \, A_{\text{eff}}^{j, \nu_f + \bar{\nu}_f}(E_\nu, \Omega) \, \Phi_{\nu_f + \bar{\nu}_f}(E_\nu, \Omega),$$

(1)

where the contribution of each neutrino flavor f to the track and shower channels is considered. Here, T^j is the livetime of the sample j reported in Table 1, Ω is the solid angle, E_ν is the neutrino energy, $A_{\text{eff}}^{j, \nu_f + \bar{\nu}_f}$ is the detector effective area, and $\Phi_{\nu_f + \bar{\nu}_f}$ is the expected flux from the source. The expected mean number of signal events for each IceCube sample $j \in [3, 7]$ given in Table 1 is calculated using Equation (1), including only the contribution of the muon flavor. Unless otherwise stated, an unbroken power-law neutrino flux is used in the analysis:

$$\Phi_{\nu_f + \bar{\nu}_f} = \Phi_0 \left(\frac{E_\nu}{1 \text{ GeV}} \right)^{-\gamma},$$

(2)

with Φ_0 being the one-flavor neutrino flux normalization. Equipartition at Earth of the three neutrino flavors is assumed.

Figure 1 shows the relative contribution of each sample as a function of the source decl. for the unbroken $E_\nu^{-\gamma}$ spectrum for two values of the spectral index, $\gamma = 2.0$ and $\gamma = 2.5$. The two

spectral indices account for the value predicted by the Fermi acceleration mechanism ($\gamma = 2.0$) and for the softer best-fit spectral indices of the isotropic flux of high-energy cosmic neutrinos measured by the IceCube Collaboration; the chosen value for the soft spectral index lies between the $\gamma = 2.92$ obtained in Kopper ([2017]) and the $\gamma = 2.28$ obtained in Stettner ([2019]). For an $E_\nu^{-2.0}$ spectrum, all samples contribute significantly to most of the Southern Sky. For the softer spectrum $E_\nu^{-2.5}$, the contribution of high-energy neutrinos is lower, and therefore the relative contribution of the ANTARES sample increases.

4. Search Method

An unbinned likelihood maximization is used to identify clusters of cosmic neutrinos from point-like and extended sources over the randomly distributed atmospheric background. The likelihood describes the data in terms of signal and background probability density functions (PDFs) and is defined as:

$$L(n_s, \gamma, \alpha, \delta) = \prod_{j=1}^{7} \prod_{i=1}^{N^j} \left[\frac{n_s^j}{N^j} S_i^j(\gamma, \alpha, \delta) + \left(1 - \frac{n_s^j}{N^j}\right) B_i^j \right], \quad (3)$$

where n_s and γ are respectively the unknown total number of signal events and signal spectral index, α and δ are the unknown equatorial coordinates of the source, and S_i^j and B_i^j are the values of the signal and background PDFs for the event i in the sample j. N^j is the total number of data events in sample j, while n_s^j is the unknown number of signal events in sample j, related to n_s through the relative contribution of the given sample, $n_s^j = n_s \cdot C^j(\delta, \Phi)$.

The signal and background PDFs are given by the product of a directional and an energy-dependent term. The same definition of the ANTARES and IceCube PDFs used in the respective individual point-source analyses (Adrian-Martinez et al. [2014]; Aartsen et al. [2017c]) is employed in this search. For the IceCube samples, the spatial PDF is given by a two-dimensional Gaussian, $P_{\text{space}}^{\text{IC}} = \exp(-\Delta\Psi_i^2/2\sigma_i^2)/(2\pi\sigma_i^2)$, with $\Delta\Psi_i$ being the angular distance of the event from the source and σ_i being the angular error estimate of the event. When searching for spatially extended sources, the value of σ_i is replaced with $\sigma_{\text{eff},i} = \sqrt{\sigma_i^2 + \sigma_s^2}$, where σ_s is the extension of the source assuming a Gaussian profile. For the ANTARES samples, a spline parameterization of the point-spread function (PSF) is used as the spatial signal PDF. The PSF is derived from Monte Carlo simulations as the probability density of the angular distance between the simulated and the reconstructed neutrino direction, α, per unit solid angle Ω: $\text{PSF}(\alpha) = \frac{dP}{d\Omega} = \frac{d\alpha}{d\Omega}\frac{dP}{d\alpha} = \frac{1}{2\pi\sin\alpha}\frac{dP}{d\alpha}$. For each ANTARES event i, $\text{PSF}(\Delta\Psi_i)$ provides the PDF of reconstructing the event at an angular distance $\Delta\Psi_i$ from the source. For extended sources, the PSF is built assuming that the original direction of the events is distributed according to a Gaussian profile around the center of the source location with standard deviation given by the assumed source extension σ_s.

During the likelihood maximization, the number of signal events n_s and the signal spectral index γ are free parameters. Moreover, the position of the source is either kept fixed or fitted

within specific limits, depending on the type of search (see Section [5]).

The test statistic, Q, is defined as:

$$Q = 2(\log L(\hat{n}_s, \hat{\gamma}, \hat{\alpha}, \hat{\delta}) - \log L(n_s = 0)), \quad (4)$$

where $\hat{n}_s$, $\hat{\gamma}$, $\hat{\alpha}$, and $\hat{\delta}$ are the best-fit values that maximize the likelihood. In order to estimate the significance of any observation, the Q-value observed at the location of a fitted cluster is compared to the test statistic distribution obtained with background-only pseudoexperiments (PEs)—pseudodata sets of data randomized in time to eliminate any local clustering due to potential sources—at the corresponding decl. The fraction of background-like pseudoexperiments with a value of Q larger than the observed Q-value gives the significance (p-value) of the observation. In case many directions in the sky are observed, a trial correction must be taken into account when estimating the significance of the observation. To this purpose, the pretrial p-value is compared to the distribution of the smallest p-values found when performing the same analysis on many background-only PEs. The fraction of background-like PEs with a p-value smaller than the observed pretrial p-value gives the trial-corrected significance (posttrial p-value) of the observation.

The free parameters can vary over a certain parameter space. The spectral index γ can range between 1.0 and 4.0, as these are the limits of reasonable spectral assumptions for astrophysical particle acceleration mechanisms. The lower limit of n_s is set to 0.001 in order to have a proper estimation of the median sensitivity, i.e., the median expected 90% C.L. upper limit on the flux normalization in case of pure background. Indeed, if the lower boundary, $n_s^{\min}$, is set to $n_s^{\min} = 0$, a test statistic $Q = 0$ is obtained in more than 50% of the PEs, leading to an overestimation of the median 90% upper limit. By setting $n_s^{\min}$ slightly above 0, the test statistic Q gets negative values for underfluctuation of the signal. This makes it possible to properly calculate the median of the background Q-distribution.

To estimate the potential of the combined search to discover a neutrino source, the 5σ discovery flux, i.e., the neutrino flux needed for a 5σ discovery in 50% of the trials, is calculated for an $E_\nu^{-\gamma}$ neutrino spectrum, with γ equal to 2.0 and 2.5, as a function of the decl. The results are shown in Figure [2] in comparison to the discovery potentials from the individual IceCube and ANTARES analyses (sensitivities are shown in Figure [6]). The discovery flux improves by a factor of $\sim$2 in different regions of the Southern Sky, depending on the energy spectrum of the source, compared to the individual IceCube and ANTARES analyses. This result is consistent with the findings of the previous combined analysis (Adrian-Martinez et al. [2016]). For an $E_\nu^{-2.0}$ spectrum, the largest improvement is achieved in a region of the sky that is centered approximately at the decl. of the Galactic Center ($\sin \delta \sim -0.5$).

5. Searches and Results

Five types of searches for point-like and extended sources are performed in this analysis. In the first two searches, a scan of the full Southern Sky and of a restricted region around the Galactic Center (GC) are carried out. In the third one, the directions of a predefined list of known sources that are potential neutrino emitters are investigated. Finally, we perform
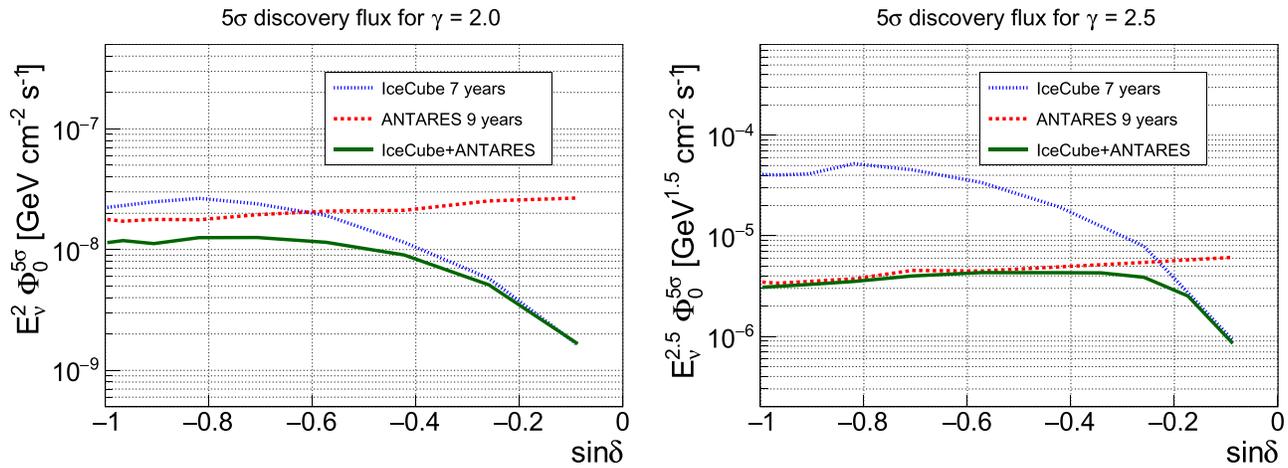
Figure 2. Point-source 5σ discovery fluxes for an unbroken $E_\nu^{-\gamma}$ neutrino spectrum, with $\gamma = 2.0$ (left) and $\gamma = 2.5$ (right). The green line indicates the results for the combined search. Blue and red curves show the results for the individual IceCube and ANTARES analyses, respectively.
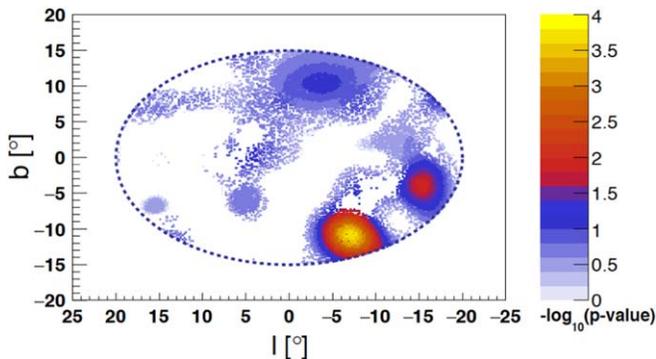

Figure 3. Sky map in galactic coordinates of the pretrial p-values obtained in the Galactic Center search for the extended source hypothesis with $\sigma_s = 2°.0$. The dashed line depicts the boundary of the search area.

two dedicated searches at the locations of two promising neutrino source candidates: the supermassive black hole (SMBH) Sagittarius A*, and the shell-type supernova remnant (SNR) RXJ 1713.7-3946.

5.1. Southern Sky Search and Galactic Center Region Search

The most significant clustering with respect to the expected background is searched for at any position in a predefined region of the sky. To find the largest deviation from background expectation, the scanned region is divided into a grid with boxes of $1° \times 1°$ in R.A. and decl. In each box, the unbinned likelihood maximization is performed, with the source position being an additional parameter that is free to vary inside the $1° \times 1°$ boundaries. For each box, the best-fit values of the number of signal events, $\hat{n}_s$, spectral index, $\hat{\gamma}$, source equatorial coordinates, $\hat{\delta}$ and $\hat{\alpha}$, and the test statistic, Q, are obtained. The direction with the smallest p-value identifies the most significant cluster of each search.

In the first search, the scanned region is defined by the whole Southern Sky. Given the large number of probed directions, the significance of weak sources is reduced due to a high trial correction. Motivated by the high concentration of candidate sources and gas around the GC and the recent observation of a possible Pevatron presence close to the GC by the HESS Collaboration (Abramowski et al. 2016), the second search is concentrated around the GC. The examined region (depicted in
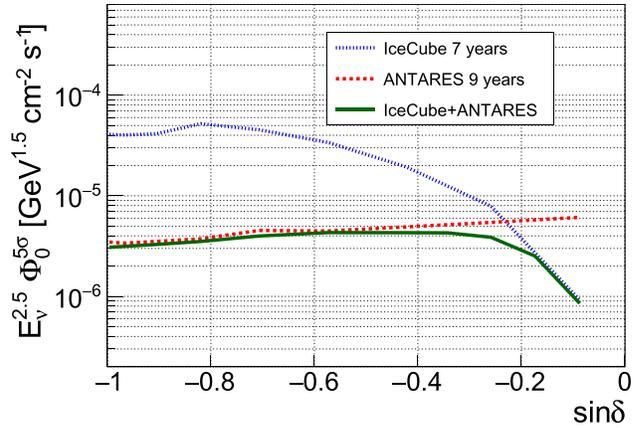
Table 2
Results of the Southern Sky Search

σ_s (°)	$\hat{n}_s$	$\hat{\gamma}$	$\hat{\delta}$ (°)	$\hat{\alpha}$ (°)	Pretrial p-value	Posttrial p-value
0.0	5.7	2.5	−40.8	213.2	1.3×10^{-5}	0.18
0.5	10.5	3.9	−22.5	18.5	3.4×10^{-5}	0.31
1.0	11.6	3.8	−21.9	18.4	8.9×10^{-5}	0.44
2.0	20.3	3.0	−40.1	274.1	2.2×10^{-4}	0.47

Note. List of the most significant clusters found when performing the Southern Sky search for different source-extension hypotheses. Reported are the source extension σ_s, the best-fit parameters (number of signal events, $\hat{n}_s$, spectral index, $\hat{\gamma}$, decl., $\hat{\delta}$, R.A., $\hat{\alpha}$), and the pretrial and posttrial p-values.

Table 3
Results of the Search in the Galactic Center Region

σ_s (°)	$\hat{n}_s$	$\hat{\gamma}$	$\hat{\delta}$ (°)	$\hat{\alpha}$ (°)	Pretrial p-value	Posttrial p-value
0.0	6.8	2.8	−42.3	273.0	7.3×10^{-4}	0.40
0.5	8.4	2.8	−42.0	273.1	5.2×10^{-4}	0.19
1.0	12.1	2.9	−41.8	274.1	6.9×10^{-4}	0.15
2.0	20.3	3.0	−40.1	274.1	2.2×10^{-4}	0.03

Note. List of the most significant clusters found when performing the search in the Galactic Center region for different source-extension hypotheses. Reported are the source extension σ_s, the best-fit parameters (number of signal events, $\hat{n}_s$, spectral index, $\hat{\gamma}$, decl., $\hat{\delta}$, R.A., $\hat{\alpha}$), and the pretrial and posttrial p-values.

Figure 3) is defined by an ellipse centered in the origin of the galactic coordinate system $(\alpha, \delta) = (266°.40, -28°.94)$.

The results are presented in Tables 2 and 3. In both cases, searches for emission regions assumed as point-like ($\sigma_s = 0°.0$) or extended ($\sigma_s = 0°.5, 1°.0, 2°.0$) are performed. For each search and source-extension hypothesis, the best-fit values of the parameters and the p-value of the most significant cluster are reported. The largest excess above background in the whole Southern Sky is found at equatorial coordinates $(\hat{\alpha}, \hat{\delta}) = (213°.2, -40°.8)$, for a point-like source hypothesis, with best-fit $\hat{n}_s = 5.7$ and $\hat{\gamma} = 2.5$. A pretrial p-value of 1.3×10^{-5} is obtained for this cluster. The corresponding posttrial significance is 18% (0.9σ in the one-sided sigma convention). Figure 4 depicts the pretrial p-values for all the
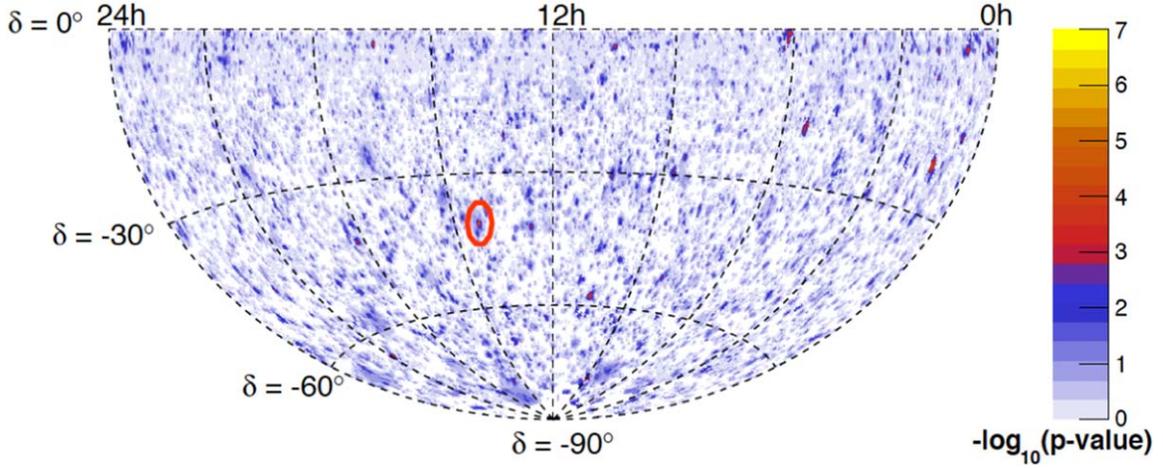
Figure 4. Sky map in equatorial coordinates of the pretrial *p*-values obtained in the Southern Sky search for the point-like source hypothesis. The red contour indicates the location of the most significant cluster.
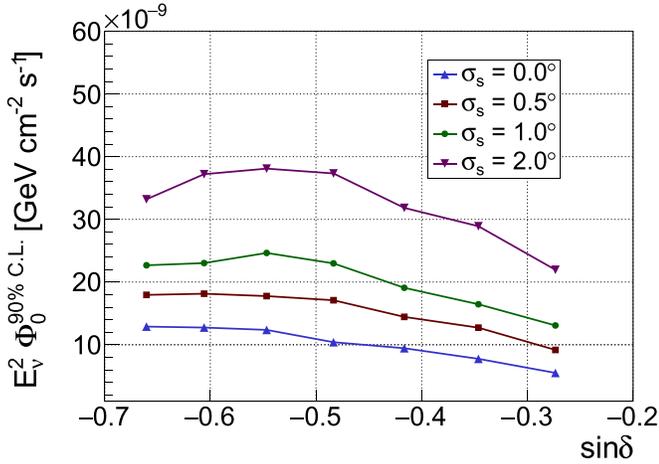

Figure 5. The 90% C.L. upper limits on the one-flavor neutrino flux normalization of the Galactic Center region search, assuming an $E_\nu^{-2.0}$ spectrum for different source extensions σ_s.

investigated directions for a point-like source hypothesis. The position of the most significant cluster is also indicated.

The most significant result of the search restricted to the Galactic Center region is observed for an extended source hypothesis ($\sigma_s = 2°0$) at equatorial coordinates $(\hat{\alpha}, \hat{\delta}) = (274°1, -40°1)$, and galactic coordinates $(\hat{l}, \hat{b}) = (-6°7, -11°0)$. The values of the best-fit $\hat{n}_s$ and $\hat{\gamma}$ are 20.3 and 3.0, respectively. The posttrial significance is 3% (1.9σ in the one-sided sigma convention). Figure 3 shows the pretrial *p*-values for the investigated directions in the Galactic Center region for an extended source hypothesis with $\sigma_s = 2°0$. The decl.-dependent 90% C.L. upper limits on the one-flavor neutrino flux normalization of this search are shown in Figure 5 for different source extensions. In this analysis, the Neyman method (Neyman 1937) is used to derive sensitivities and limits.

5.2. Candidate List Search

In this study, the location of 57 astrophysical objects is investigated to look for point-like emission of high-energy neutrinos. The candidates are sources of high-energy γ-rays and belong to different object classes. The analyzed candidates

correspond to all the sources in the Southern Sky considered in the candidate list search performed by the ANTARES (Adrian-Martinez et al. 2014) and the IceCube (Aartsen et al. 2017c) Collaborations. Here, only the number of signal events and the spectral index are left as free parameters in the likelihood maximization, as the direction of the selected sources is known. The list of the astronomical candidates is shown in Table 4, together with their equatorial coordinates, fitted number of signal events, fitted spectral index, pretrial *p*-value, and 90% C.L. upper limits on the one-flavor neutrino flux normalization for an $E_\nu^{-2.0}$ and an $E_\nu^{-2.5}$ spectrum. Figure 6 shows the 90% C.L. upper limits as a function of the source decl. together with the median sensitivity.

The most significant source of the list is HESSJ1023-575, a TeV γ-ray source coincident with the young stellar cluster Westerlund 2 (Aharonian 2007), with a pretrial *p*-value of 0.79%. A total of 6.4 signal events and a spectral index of 3.5 are fitted for the cluster at the position of HESSJ1023-575. The trial-corrected significance of the cluster is 42%, corresponding to 0.2σ in the one-sided convention. The second- and third-most significant sources are PKS1440-389 and HESSJ1458-608, with respective *p*-values of 0.85% and 3.6%.

5.3. Sagittarius A*

Sagittarius A*, the SMBH located at the center of our Galaxy, $(\alpha, \delta) = (266°42, -29°01)$, is a candidate source of particular interest. Indeed, the surroundings of this kind of black hole are highly plausible acceleration sites of very-high-energy cosmic rays, and therefore are possible sources of cosmic neutrinos (Bai et al. 2014; Fang & Murase 2018). The high density of candidate objects and the presence of molecular clouds around the Galactic Center makes the detection of an extended source more likely than the detection of a point-like source. For these reasons, a search for astrophysical neutrinos from Sagittarius A* and nearby objects is carried out by testing the point-like ($\sigma_s = 0°0$) and extended source ($\sigma_s = 0°5, 1°0, 2°0$) hypotheses. The values of the best-fit parameters at the investigated location for the various tested source extensions are presented in Table 5, together with the observed *p*-value. The largest excess above the background is found for a point-like source hypothesis, with best-fit $\hat{n}_s = 2.9$ and $\hat{\gamma} = 2.1$, and a significance of 6% (1.6σ in the one-sided sigma convention). The 90% C.L. upper limits on the one-flavor

Table 4
Results of the Candidate List Search

Name	δ (°)	$\sin\delta$	α (°)	$\hat{n}_s$	$\hat{\gamma}$	p-value	$\Phi_{0,\gamma=2.0}^{90\%\ C.L.}$ ζ[a]	$\Phi_{0,\gamma=2.5}^{90\%\ C.L.}$ χ[b]
LHA120-N-157B	−69.16	−0.93	84.43	…	…	…	3.6	0.9
HESSJ1356-645	−64.50	−0.90	209.00	1.2	3.1	0.18	6.2	1.4
PSRB1259-63	−63.83	−0.90	195.70	1.3	4.0	0.19	6.2	1.5
HESSJ1303-631	−63.20	−0.89	195.74	…	…	…	3.7	0.9
RCW86	−62.48	−0.89	220.68	1.0	1.6	0.20	6.3	1.5
HESSJ1507-622	−62.34	−0.89	226.72	…	…	…	3.7	1.0
HESSJ1458-608	−60.88	−0.87	224.54	3.7	3.6	0.036	9.3	2.0
ESO139-G12	−59.94	−0.87	264.41	…	…	…	3.7	1.0
MSH15-52	−59.16	−0.86	228.53	…	…	…	3.7	1.0
HESSJ1503-582	−58.74	−0.85	226.46	…	…	…	3.7	1.0
HESSJ1023-575	−57.76	−0.85	155.83	6.4	3.5	0.0079	11.2	2.5
CirX-1	−57.17	−0.84	230.17	…	…	…	3.8	1.0
SNRG327.1-01.1	−55.08	−0.82	238.65	…	…	…	3.8	1.0
HESSJ1614-518	−51.82	−0.79	243.58	1.6	4.0	0.21	6.1	1.6
HESSJ1616-508	−50.97	−0.78	243.97	2.0	2.0	0.18	6.5	1.6
PKS2005-489	−48.82	−0.75	302.37	0.4	2.9	0.18	6.4	1.6
GX339-4	−48.79	−0.75	255.70	…	…	…	3.7	1.1
HESSJ1632-478	−47.82	−0.74	248.04	…	…	…	3.7	1.1
RXJ0852.0-4622	−46.37	−0.72	133.00	…	…	…	3.7	1.1
HESSJ1641-463	−46.30	−0.72	250.26	…	…	…	3.7	1.1
VelaX	−45.60	−0.71	128.75	…	…	…	3.6	1.1
PKS0537-441	−44.08	−0.70	84.71	1.6	2.2	0.098	7.2	1.9
CentaurusA	−43.02	−0.68	201.36	…	…	…	3.6	1.1
PKS1424-418	−42.10	−0.67	216.98	0.6	2.3	0.24	5.5	1.6
RXJ1713.7-3946	−39.75	−0.64	258.25	…	…	…	3.5	1.2
PKS1440-389	−39.14	−0.63	220.99	3.0	2.4	0.0085	10.8	3.0
PKS0426-380	−37.93	−0.61	67.17	…	…	…	3.5	1.2
PKS1454-354	−35.67	−0.58	224.36	3.9	2.1	0.089	7.3	2.1
PKS0625-35	−35.49	−0.58	96.78	…	…	…	3.4	1.2
TXS1714-336	−33.70	−0.55	259.40	1.2	2.3	0.17	5.9	1.9
SwiftJ1656.3-3302	−33.04	−0.55	254.07	2.8	2.1	0.15	6.1	1.9
PKS0548-322	−32.27	−0.53	87.67	…	…	…	3.2	1.2
H2356-309	−30.63	−0.51	359.78	…	…	…	3.0	1.2
PKS2155-304	−30.22	−0.50	329.72	…	…	…	3.0	1.2
HESSJ1741-302	−30.20	−0.50	265.25	1.0	2.9	0.12	6.0	2.0
PKS1622-297	−29.90	−0.50	246.50	4.4	1.9	0.048	7.4	2.4
Sagittarius A*	−29.01	−0.48	266.42	2.9	2.1	0.06	7.2	2.4
Terzan5	−24.90	−0.42	266.95	…	…	…	2.5	1.2
1ES1101-232	−23.49	−0.40	165.91	…	…	…	2.4	1.2
PKS0454-234	−23.43	−0.40	74.27	…	…	…	2.4	1.2
W28	−23.34	−0.40	270.43	1.7	2.5	0.094	4.9	2.0
PKS1830-211	−21.07	−0.36	278.42	…	…	…	2.2	1.2
NRG015.4+00.1	−15.47	−0.27	274.52	…	…	…	1.6	1.0
LS5039	−14.83	−0.26	276.56	…	…	…	1.5	1.0
QSO1730-130	−13.10	−0.23	263.30	…	…	…	1.3	0.9
HESSJ1826-130	−13.01	−0.23	276.51	…	…	…	1.3	0.8
HESSJ1813-126	−12.68	−0.22	273.34	…	…	…	1.3	0.8
1ES0347-121	−11.99	−0.21	57.35	…	…	…	1.2	0.8
PKS0727-11	−11.70	−0.20	112.58	2.5	2.7	0.13	2.1	1.2
HESSJ1828-099	−9.99	−0.17	277.24	2.4	2.9	0.079	2.0	1.2
HESSJ1831-098	−9.90	−0.17	277.85	…	…	…	0.9	0.6
HESSJ1834-087	−8.76	−0.15	278.69	…	…	…	0.8	0.5
PKS1406-076	−7.90	−0.14	212.20	6.8	2.7	0.11	1.5	0.7
QSO2022-077	−7.60	−0.13	306.40	…	…	…	0.7	0.4
HESSJ1837-069	−6.95	−0.12	279.41	2.5	3.4	0.24	1.0	0.5
2HWCJ1309-054	−5.49	−0.10	197.31	9.1	3.2	0.051	0.9	0.3
3C 279	−5.79	−0.10	194.05	2.5	2.2	0.28	0.6	0.3

Notes. List of astrophysical objects analyzed in the candidate list search. Reported are the source's name, equatorial coordinates, best-fit values of the free parameters, pretrial p-value and 90% C. L. upper limits on the one-flavor neutrino flux normalization for an $E_\nu^{-2.0}$ spectrum, $\Phi_{0,\gamma=2.0}^{90\%\ C.L.}$ (in units of 10^{-9} GeV^{-1} cm^{-2} s^{-1}), and for an $E_\nu^{-2.5}$ spectrum, $\Phi_{0,\gamma=2.5}^{90\%\ C.L.}$ (in units of 10^{-6} GeV^{-1} cm^{-2} s^{-1}). Dots (...) in the fitted number of source events, spectral index and pretrial p-value indicate sources with null observations ($\hat{n}_s = 0.001$).
[a] $\zeta = 10^{-9}$ GeV^{-1} cm^{-2} s^{-1}.
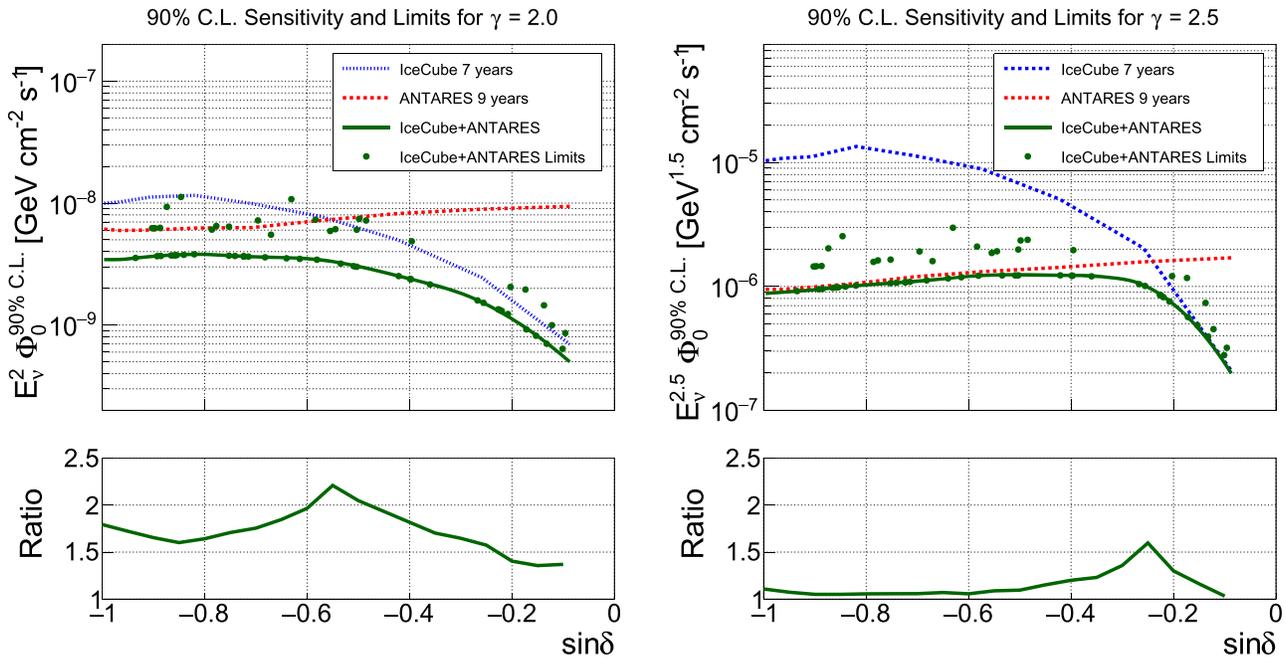[b] $\chi = 10^{-6}$ GeV^{-1} cm^{-2} s^{-1}.

Figure 6. Top: upper limits at 90% C.L. on the one-flavor neutrino flux normalization from the analyzed candidates (green dots) reported in Table 4 as a function of the source decl. An unbroken $E_\nu^{-\gamma}$ neutrino spectrum is assumed, with $\gamma = 2.0$ (left) and $\gamma = 2.5$ (right). The green line indicates the sensitivity of the combined analysis. The dashed curves indicate the sensitivities for the IceCube (blue) and ANTARES (red) individual analyses. Bottom: ratio between the best individual sensitivity and the combined sensitivity as a function of the source decl. for the spectral indices $\gamma = 2.0$ (left) and $\gamma = 2.5$ (right).

Table 5
Results of the Search at the Location of Sagittarius A*

σ_s (°)	$\hat{n}_s$	$\hat{\gamma}$	p-value
0.0	2.9	2.1	0.06
0.5	0.6	2.0	0.26
1.0	…	…	…
2.0	0.3	3.8	0.40

Note. Values of the best-fit parameters (number of signal events, $\hat{n}_s$, and spectral index, $\hat{\gamma}$) and p-value for the search at the location of Sagittarius A* for different hypotheses of source extension σ_s. Dots (...) in the fitted number of source events, spectral index, and p-value indicate cases of null observations ($\hat{n}_s = 0.001$).

neutrino flux normalization as a function of the source extension are shown in Figure 7, together with the median sensitivity and the discovery flux.

5.4. RXJ 1713.7-3946

SNRs are the prime candidates for the acceleration of Galactic cosmic rays, and hence are potential sources of astrophysical neutrinos. In the past years, a large number of Galactic SNRs have been identified by γ-ray telescopes.[105] Some of the observed γ-ray spectra extend up to tens of TeV, suggesting that these objects are accelerators of high-energy particles. The observation of neutrinos from these sources would be an unambiguous indication of hadronic acceleration. The shell-type SNR RXJ 1713.7-3946, at equatorial coordinates $(\alpha, \delta) = (258°.25, -39°.75)$, is the brightest object of this kind in the TeV γ-ray sky and represents a particularly interesting target to the search for cosmic neutrinos

---
[105] http://tevcat.uchicago.edu
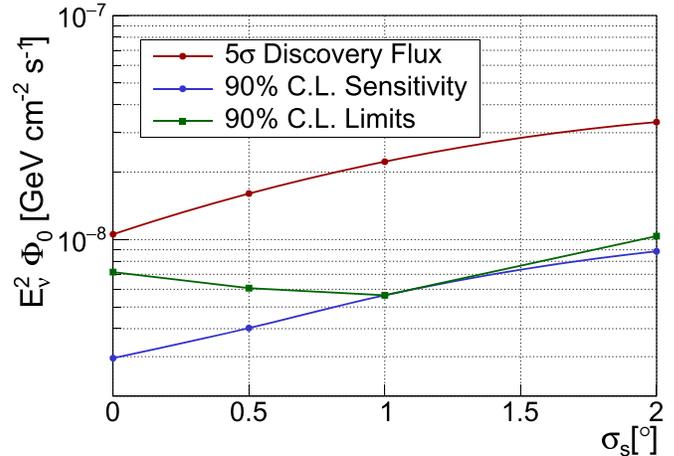
Figure 7. Discovery flux (red dots), median sensitivity (blue dots) and 90% C. L. upper limits (green squares) for the search at the location of Sagittarius A*, assuming an $E_\nu^{-2.0}$ spectrum, as a function of the angular extension σ_s.

(Vissani 2006; Kappes et al. 2007; Morlino et al. 2009). In this analysis, two different models are considered for the neutrino emission: that proposed by Kappes et al. (2007), in the following indicated as RXJ 1713.7-3946 (1), and the one recently introduced for KM3NeT neutrino source search estimations (Aiello et al. 2019) and based on the methods described by Vissani et al. (Vissani 2006; Villante & Vissani 2008; Vissani & Villante 2008), hereafter referred to as RXJ 1713.7-3946 (2). Both models describe a neutrino spectrum of the form of:

$$\Phi_{\nu_f + \bar{\nu}_f} = \Phi_0 \left(\frac{E_\nu}{1\ \text{TeV}} \right)^{-\Gamma} \exp[-(E_\nu/E_{\text{cut}})^\beta], \qquad (5)$$

<div align="center">

Table 6
Results of the Search at the Location of RXJ 1713.7-3946

</div>

Spectrum	Φ_0 ξ[a]	Γ	E_{cut} (TeV)	β	$\hat{n}_s$	p-value	$\Phi_{sens}^{90\%C.L.}/\Phi_0$	$\Phi_{UL}^{90\%C.L.}/\Phi_0$
RXJ 1713.7-3946 (1)	1.55	1.72	1.35	0.5	0.3	0.40	10.7	13.2
RXJ 1713.7-3946 (2)	0.89	2.06	8.04	1	0.3	0.41	9.7	11.7

Notes. List of considered neutrino emission models for the search at the location of RXJ 1713.7-3946 and respective results. For each model, the values of the neutrino spectrum parameters, Φ_0, Γ, E_{cut}, and β entering Equation (5) are provided. The last four columns show the results in terms of best-fit number of signal events, $\hat{n}_s$, p-value, ratio of the sensitivity to the assumed source flux, $\Phi_{sens}^{90\%C.L.}/\Phi_0$, and ratio of the upper limit to the assumed source flux, $\Phi_{UL}^{90\%C.L.}/\Phi_0$.
[a] $\xi = 10^{-11}\,\mathrm{TeV^{-1}\,cm^{-2}\,s^{-1}}$.

where E_ν is the neutrino energy and the values of the neutrino spectrum parameters Φ_0, Γ, E_{cut}, and β are listed in Table 6. A Gaussian extension with $\sigma_s = 0°.6$ is assumed for the source as reported by the γ-ray analysis performed by the H.E.S.S. Collaboration (Abdalla et al. 2018).

No significant evidence of astrophysical neutrinos from the direction of the SNR is observed for either of the considered spectra. The fitted number of signal events and the p-value observed at the source position are presented in Table 6 for each spectrum hypothesis, together with the 90% C.L. sensitivity and upper limit, both expressed as a ratio with the theoretical source flux.

6. Conclusions

A combined search for neutrino sources in the Southern Sky using data from the ANTARES and IceCube telescopes was presented. Neither significant point-like nor extended neutrino emission over the background expectation was found.

The largest excess over the whole Southern Sky, with a posttrial significance of 18%, was found at equatorial coordinates $(\hat{\alpha}, \hat{\delta}) = (213°.2, -40°.8)$, for a point-like source hypothesis. When limiting the search to the GC region, the most significant cluster was found at equatorial coordinates $(\hat{\alpha}, \hat{\delta}) = (274°.1, -40°.1)$, with a posttrial significance of 3%, for a source extension of $2°.0$. Upper limits on the neutrino flux from 57 astrophysical candidate sources were presented. The most significant source candidate is HESSJ1023-575, with a posttrial significance of 42%. The upper limits on the flux from HESSJ1023-575 were set to $1.1 \times 10^{-8}(2.5 \times 10^{-6})$ in units of $\mathrm{GeV^{-1}cm^{-2}s^{-1}}$ for an unbroken power-law spectrum with spectral index $\gamma = 2.0$ ($\gamma = 2.5$). Sagittarius A* was tested as a point-like source and as an extended source. The largest excess over the background was observed at an angular extension of $0°.0$ with a significance of 6%. Finally, the location of the SNR RXJ 1713.7-3946 was investigated assuming two proposed neutrino emission models and a source extension of $0°.6$. As no significant evidence of cosmic neutrinos was observed, upper limits were derived.

This analysis shows the strong potential to search for neutrino sources in the Southern Sky using the joint data sets of the ANTARES and IceCube telescopes. The combination of the two detectors, which differ in size and location, allows for an improvement of up to a factor of ∼2 in the sensitivity in different regions of the Southern Sky, depending on the energy spectrum of the source. For a soft spectral index, the contribution of high-energy neutrinos is suppressed and ANTARES dominates in most of the Southern Sky. The complementarity of the two detectors is mostly effective for a harder spectral index, as all the samples provide a significant contribution. For an $E_\nu^{-2.0}$ spectrum, a considerable gain in the sensitivity to point-like sources is achieved in all the Southern Sky and in a larger scale in the region close to the Galactic Center.

ORCID iDs

B. Baret https://orcid.org/0000-0001-6064-3858
G. Illuminati https://orcid.org/0000-0002-4138-8027
O. Kalekin https://orcid.org/0000-0001-6206-1288
U. Katz https://orcid.org/0000-0002-7063-4418
R. Le Breton https://orcid.org/0000-0001-8522-4983
E. Leonora https://orcid.org/0000-0002-0536-3551
J. Wilms https://orcid.org/0000-0003-2065-5410
A. Franckowiak https://orcid.org/0000-0002-5605-2219
J. Gallagher https://orcid.org/0000-0001-8608-0408
S. Garrappa https://orcid.org/0000-0003-2403-4582
M. Santander https://orcid.org/0000-0001-7297-8217
N. L. Strotjohann https://orcid.org/0000-0002-4667-6730

References

Aartsen, M. G., Abraham, K., Ackermann, M., et al. 2016, ApJ, 833, 3
Aartsen, M. G., Abraham, K., Ackermann, M., et al. 2017a, ApJ, 835, 45
Aartsen, M. G., Abraham, K., Ackermann, M., et al. 2017c, ApJ, 835, 151
Abdalla, H., Abramowski, A., Aharonian, F., et al. 2018, A&A, 612, A6
Aartsen, M. G., Ackermann, M., Adams, J., et al. 2014, PhRvL, 113, 101101
Aartsen, M. G., Ackermann, M., Adams, J., et al. 2015, ApJ, 807, 46
Aartsen, M. G., Ackermann, M., Adams, J., et al. 2017b, JInst, 12, P03012
Aartsen, M. G., Ackermann, M., Adams, J., et al. 2018a, Sci, 361, 147
Aartsen, M. G., Ackermann, M., Adams, J., et al. 2018b, Sci, 361, eaat1378
Abramowski, A., Aharonian, F., Benkhali, F., et al. 2016, Natur, 531, 476
Achterberg, A., Ackermann, M., Adams, J., et al. 2006, APh, 26, 155
Adrian-Martinez, S., Albert, A., André, M., et al. 2014, ApJL, 786, L5
Adrian-Martinez, S., Albert, A., André, M., et al. 2016, ApJ, 823, 65
Ageron, M., Aguilar, J. A., Al Samarai, I., et al. 2011, NIMPA, 656, 11
Aharonian, F. 2007, A&A, 467, 1075
Aiello, S., Akrame, S. E., Ameli, F., et al. 2019, APh, 111, 100
Albert, A., André, M., Anghinolfi, M., et al. 2018, ApJL, 863, L30
Albert, A., André, M., Anghinolfi, M., et al. 2019, ApJ, 879, 108
Bai, Y., Barger, A. J., Barger, V., et al. 2014, PhRvD, 90, 063012
Becker, J. K. 2008, PhR, 458, 173
Fang, K., & Murase, K. 2018, NatPh, 14, 396
Franckowiak, A. 2017, JPhCS, 888, 012009
Gaisser, T. K., Halzen, F., & Stanev, T. 1995, PhR, 258, 173, [Erratum: 1996, PhR, 271, 355]
Haack, C., & Wiebusch, C. 2017, ICRC (Busan), 35, 1005
Halzen, F., & Hooper, D. 2002, RPPh, 65, 1025
Kappes, A., Hinton, J., Stegmann, C., & Aharonian, F. A. 2007, ApJ, 656, 870, [Erratum: 2007, ApJ, 661, 1348]
Kelner, S. R., & Aharonian, F. A. 2008, PhRvD, 78, 034013 [Erratum: 2010, PhRvD, 82, 099901]
Kopper, C. 2017, ICRC (Busan), 35, 981
Kopper, C., Giang, W., & Kurahashi, N. 2016, ICRC (The Hague), 34, 1081
Morlino, G., Amato, E., & Blasi, P. 2009, MNRAS, 392, 240
Murase, K. 2015, in AIP Conf. Proc. 1666, Proc. 26th Int. Conf. on Neutrino Physics and Astrophysics (Neutrino 2014), ed. E. Kearns & G. Feldman (Melville, NY: AIP), 040006
Neyman, J. 1937, RSPTA, A236, 333
Stettner, J. 2019, ICRC (Madison), 36, 1017
Villante, F. L., & Vissani, F. 2008, PhRvD, 78, 103007
Vissani, F. 2006, APh, 26, 310
Vissani, F., & Villante, F. L. 2008, NIMPA, 588, 123